Microscopic Theory and Simulation of Quantum-Well Intersubband Absorption

Jianzhong Li and C. Z. Ning

Center for Nanotechnology and NASA Advanced Supercomputing Division
NASA Ames Research Center, Mail Stop N229-1, Moffett Field, CA 94035-1000

ABSTRACT

We study the linear intersubband absorption spectra of a 15 nm InAs quantum well using the intersubband semiconductor Bloch equations with a three-subband model and a constant dephasing rate. We demonstrate the evolution of intersubband absorption spectral line shape as a function of temperature and electron density. Through a detailed examination of various contributions, such as the phase space filling effects, the Coulomb many-body effects and the nonparabolicity effect, we illuminate the underlying physics that shapes the spectra.

Keywords: Intersubband transition, linear absorption, semiconductor heterostructure, InAs quantum well

1. INTRODUCTION

Study of semiconductor optoelectronic devices in the infrared regime attracts great attention owing to their applications in communications, sensing, imaging, and "finger printing" molecules. Current efforts of extending the spectral range of available light sources and detectors toward long micrometer wavelength regime involve very diverse device concepts and designs, such as quantum cascade lasers and type II interband lasers.[1] One of the promising device designs for achieving longwave infrared, or far-infrared lasing is based on optically pumped intersubband transitions (ISBTs).[2] The advantages of this concept include large dipole matrix elements and ultrafast dynamic response. Such design could be made even more attractive if material systems with deeper quantum wells (QWs) are adopted, such as the InGaAs/AlAsSb QWs, since then the pumping source for such systems could be another compact semiconductor diode laser.[3] In this respect, the antimonide-based QWs offer an interesting alternative, as the conduction band offset of InAs/AlSb heterostructure is as deep as 2 eV, providing more design flexibilities.

We have investigated effects of bandstructure, Coulomb interaction, electron-longitudinal optical (LO) phonon interaction, and other material-related issues on ISBTs within a two-subband model.[4–7] The analysis is based on density matrix formalism. In this paper, linear intersubband absorption spectra in a 15 nm InAs quantum well are studied in the same framework—the intersubband semiconductor Bloch equations approach—but under a three-subband model and dephasing rate approximation. We demonstrate the evolution of intersubband absorption line shape as temperature and carrier density are changed. Through a detailed examination of various contributions, such as phase space filling effects and Coulomb interaction-induced many-body effects, we elucidate the underlying physics that shapes the spectra.

Theoretical treatment of intersubband transitions typically involves two steps. The first step is to compute the bandstructure, while the second step is to formulate light-semiconductor interaction on the basis of this obtained bandstructure. The first step is sometimes called determination of the ground state, while the second step treats the excitations of the system by external light field. In the present model study, we model the bandstructure with different effective masses for the three parabolic subbands, whereas the density matrix theory[8,9] is adopted to treat the light-semiconductor heterostructure interaction. By explicitly formulating the two-point correlation functions, such as the intersubband polarization, the set of the so-called intersubband semiconductor Bloch equations (iSBEs) is derived. Within this approach, it is known that the exchange interaction leads to

Further author information: Both authors are employees of Computer Sciences Corporation.
J.L.: E-mail: jianzhng@nas.nasa.gov, Telephone: (650) 604 4410
C.Z.N.: E-mail: cning@mail.arc.nasa.gov, Telephone: (650) 604 3983

a self-energy renormalization (exchange self-energy, or XSE) to the single particle energy and a nonlocal vertex (excitonlike in the case of interband transitions) term that couples the other intersubband polarizations to each individual $\boldsymbol{k}$-transition, whereas the direct (Hartree) interaction contributes the so-called depolarization field term that describes the dynamic screening of the charge carriers to the external exciting field, which is of collective nature and modifies the local field that each individual carrier feels. This paper detailedly examines the case of a 15 nm InAs quantum well within a three-subband model and illustrates how different contributions help shape the ISBTs as a finction of temperature and carrier density.

This paper is organized as follows: In the second section, we summarize our theoretical considerations with a minimum set of equations; we present simulated ISBT spectra for the InAs quantum well in Sec. 3; and then we conclude the paper with a summary.

2. THEORETICAL CONSIDERATIONS

As mentioned above the microscopic theory consists of two steps: the static description of the subband dispersions and kinetic description for the intersubband optical transitions. We describe the energy dispersions in an approximate manner in this work, or more specifically, different effective masses are used for the three subbands. The focus of our work is on the kinetic description of the ISBTs.

To treat the light-semiconductor heterostructure interaction, we consider the following expectation values of the bilinear combination of creation ($c^{\dagger}_{n\boldsymbol{k}}$) and annihilation ($c_{n\boldsymbol{k}}$) operators among the same $\boldsymbol{k}$ (the in-plane electron wavevector) states within a three-subband model (subband labeled by index $n = 1, 2, 3$): ground subband population $f_{1\boldsymbol{k}} \equiv \langle c^{\dagger}_{1\boldsymbol{k}} c_{1\boldsymbol{k}} \rangle$, lower excited subband population $f_{2\boldsymbol{k}} \equiv \langle c^{\dagger}_{2\boldsymbol{k}} c_{2\boldsymbol{k}} \rangle$, upper excited subband population $f_{3\boldsymbol{k}} \equiv \langle c^{\dagger}_{3\boldsymbol{k}} c_{3\boldsymbol{k}} \rangle$, intersubband polarization $p^{12}(\boldsymbol{k}) \equiv \langle c^{\dagger}_{1\boldsymbol{k}} c_{2\boldsymbol{k}} \rangle$ between subband 1 and 2, $p^{23}(\boldsymbol{k}) \equiv \langle c^{\dagger}_{2\boldsymbol{k}} c_{3\boldsymbol{k}} \rangle$ between subband 2 and 3, $p^{13}(\boldsymbol{k}) \equiv \langle c^{\dagger}_{1\boldsymbol{k}} c_{3\boldsymbol{k}} \rangle$ between subband 1 and 3, and their corresponding Hermitian conjugates. Following the quantum kinetic approach, the semiclassical kinetic equations for the above dynamic variables are derived as a limiting case.[9] The derivation is extensive and will not be given here. The resultant equations (only the ones for intersubband polarizations here), under linearization with respect to the incident light field amplitude, some plausible assumptions, and the rotating wave approximation, are found as follows:

$$\left[\hbar\left(\omega + i\gamma_p^{mn}\right) - \left(\varepsilon_{n\boldsymbol{k}} - \varepsilon_{m\boldsymbol{k}}\right)\right] p_{\boldsymbol{k}}^{mn} = \left(\boldsymbol{d}_{\boldsymbol{k}}^{mn} \cdot \boldsymbol{E}_0 + \varepsilon_{\boldsymbol{k}}^{mn}\right)\left(f_{m\boldsymbol{k}} - f_{n\boldsymbol{k}}\right) - \sum_{j,\boldsymbol{q}} f_{j\boldsymbol{k}+\boldsymbol{q}}\left(V_{\boldsymbol{q}}^{njlj} p_{\boldsymbol{k}}^{ml} - V_{\boldsymbol{q}}^{ljmj} p_{\boldsymbol{k}}^{ln}\right) , \quad (1)$$

where ω is the angular frequency of the incident light of amplitude $\boldsymbol{E}_0$, γ_p^{mn} is the dephasing rate, $\boldsymbol{d}_{\boldsymbol{k}}^{mn}$ is the dipole matrix element, and $l \neq m$, $l \neq n$. $f_{m\boldsymbol{k}}$ is taken as the Fermi distribution function in the linear absorption calculation and $p_{\boldsymbol{k}}^{mn}$ is the amplitude of the intersubband polarization $p^{mn}(\boldsymbol{k})$. The renormalized single particle energy ($\varepsilon_{m\boldsymbol{k}}$) by the Coulomb self-energy and the *local field* correction term ($\varepsilon_{\boldsymbol{k}}^{mn}$) are, respectively, given by

$$\varepsilon_{m\boldsymbol{k}} = E_{m\boldsymbol{k}}^{(0)} - \sum_{l,\boldsymbol{q}} V_{\boldsymbol{q}}^{mlml} f_{l\boldsymbol{k}+\boldsymbol{q}} , \quad (2)$$

$$\varepsilon_{\boldsymbol{k}}^{mn} = -\sum_{j\neq l,\boldsymbol{q}} V_{\boldsymbol{q}}^{njml} p_{\boldsymbol{k}+\boldsymbol{q}}^{jl} + \sum_{j\neq l,\boldsymbol{q}} V_{\boldsymbol{0}}^{njlm} p_{\boldsymbol{q}}^{jl} . \quad (3)$$

The *local field* correction consists of a Fock (first) term that gives rise to a type of collective excitation called the repellon and a Hartree (second) term that stimulates another type of collective excitation called the intersubband plasmons (ISPs).[6,10] We mention that the first term is responsible for the Fermi-edge singularity effect, whereas the remaining term leads to the depolarization effect, as described detailedly in our earlier work. Their effects have been known from previous studies and play the same roles as well within the present three-subband model. The Coulomb matrix elements ($V_{\boldsymbol{q}}^{njml}$'s) are defined as in Ref..[5] The static single plasmon-pole approximation[8] has been used for screening the exchange interaction by the intrasubband processes in the present simulation work. The iSBEs are solved numerically by a matrix inversion for the intersubband polarization functions. We note that the last term in Eq. (1) is unimportant in this work.

The linear absorption coefficient is defined by

$$\alpha(\omega) \equiv \frac{\omega}{\varepsilon_0 n(\omega) c}\mathcal{I}m\{\epsilon(\omega)\} \approx \frac{\omega}{n(\omega)c}\mathcal{I}m\{\chi(\omega)\} , \quad (4)$$

with $n(\omega)$ being the background index of refraction (slowly varying in frequency), $\epsilon(\omega)$ the dielectric function, and c the speed of light *in vacuo*. The susceptibility, $\chi(\omega)$, is given by

$$\chi(\omega) \equiv P/\varepsilon_0 E_0 \,, \tag{5}$$

$$P = 2S/[(2\pi)^2 \mathcal{V}] \sum_{m \neq n} \int d\boldsymbol{k} \, \{d_{\boldsymbol{k}}^{mn}\}^* p_{\boldsymbol{k}}^{mn} \,. \tag{6}$$

where P is the total intersubband polarization, ε_0 is the electric constant, S is the QW area, and $\mathcal{V}$ is the QW volume. $\mathcal{V} = WS$, and W is the QW thickness. Finally, the absorbance of the semiconductor heterostructure is given by $2W\alpha(\omega)$ (per bounce at full TM polarization).

3. NUMERICAL RESULTS

Table I lists the bandstructure-related parameter values that were used in the numerical simulation. All the values were obtained using the spurious-state-free 8-band $\boldsymbol{k} \cdot \boldsymbol{p}$ Hamiltonian under the envelope function approximation,[5,11] with the exception of the depolarization factors. Their values are the quantum box results of the same QW thickness. In order for data integrity, the calculated subband populations are also presented here in Table II, which are auxillary to the understanding of the simulated spectra, as shown later.

Table I. Parameters used in simulations

subband effective mass	m_i (m_e)	0.0336 (1)	0.049 (2)	0.0715 (3)	
subband separation	E_{ij} (meV)	131.065 (12)	150.92 (23)	281.985 (13)	
dipole matrix element	d^{ij} (e·Å)	30.0 (12)	35.0 (23)	0.0 (13)	
depolarization factor	D^{jlmn} (W)	0.1222 (1122)	0.1146 (2233)	0.0343 (1133)	0.1101 (1232)

m_e: free electron mass; e: absolute electron charge. Numbers in parenthesis after entry values indicate subband indices. See Ref.[10] for definition of the depolarization factor.

The effective masses were found after a least square fitting to the $\boldsymbol{k} \cdot \boldsymbol{p}$ subbands; the subband separation is the energy difference at the Γ point ($\boldsymbol{k} = \boldsymbol{0}$) between the $\boldsymbol{k} \cdot \boldsymbol{p}$ subbands; the dipole matrix elements are found to be weakly dependent on the wavevector so that their values at the Γ point were used in the simulation. We mention that the depolarization factor is a measure of the contributing strength of the Hartree term to the *local field*, which in turn determines the strength of the ISPs.[6,10] Note that a value of the order of 0.1, in the unit of the QW thickness (W), means a rather strong depolarization effect; the total strength of the depolarization effect is proportional to the product of the QW thickness and the density difference between the subbands. Furthermore, coherent Coulomb effects due to the coupling of ISPs associated with individual ISBTs are important, and the results will be presented elsewhere.

Table II. Calculated subband populations

electron density (10^{12} cm^{-2})	temperature (K)	n_1	n_2	n_3
1.00	12	1.00	0.00	0.00
	80	1.00	2.41×10^{-5}	1.09×10^{-14}
	300	9.58×10^{-1}	4.16×10^{-2}	1.84×10^{-4}
2.50	12	2.11	3.92×10^{-1}	0.00
	80	2.10	3.95×10^{-1}	9.91×10^{-10}
	300	2.00	4.96×10^{-1}	3.49×10^{-3}
5.00	12	3.13	1.87	0.00
	80	3.13	1.87	3.77×10^{-5}
	300	3.09	1.84	6.78×10^{-2}
7.50	12	4.06	3.23	2.10×10^{-1}
	80	4.04	3.21	2.49×10^{-1}
	300	3.93	3.06	5.10×10^{-1}

n_i: Electron density in Subband i.

Shown in Fig. 1 are the energy dispersions of the considered three conduction subbands (left panel) and the single-particle absorption spectrum (right panel) of the 15 nm InAs QW. Owing to a nonparabolicity of the bulk InAs conduction band, dispersions for the three subbands are different; the subband separations are k-dependent. The rather strong nonparabolicity of InAs leads to a large value range of the intersubband separation. In a single-particle picture, this introduces an inhomogeneous broadening and an accompanying low frequency tailing to the absorption spectrum. All these are reflected in the figure. Note that we did not consider the temperature dependence of the subband strucuture in this model study. Also shown in the figure, as a comparison, is the case of vanishing nonparabolicity (dotted curves with upward arrows): The spectrum consists of sharp resonances without any inhomogeneous broadening.

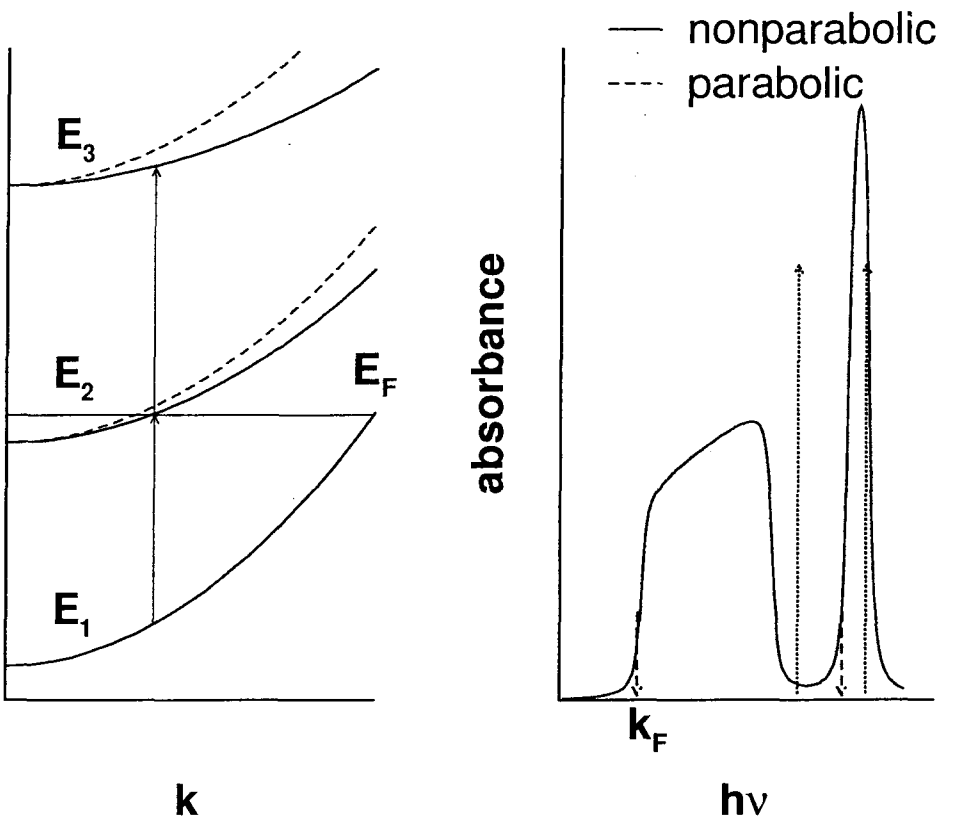

Figure 1. Schematic of subband dispersions (left panel) and single-particle intersubband absorption spectrum for a 15 nm InAs quantum well. The decreasing intersubband separation with increasing k represents the result of nonparabolicity in InAs conduction band, which is consequently and unambiguously reflected by the broadened absorption spectrum.

As outlined in Sec. 2, the matrix inversion method was used to solve Eq. (1) for the intersubband polarization functions. Then the absorbance was calculated using these functions according to Eqs. (4)–(6) and the results are presented in Figs. 2–4. We first show how the absorbance changes as a function of temperature at different electron densities in Fig. 2. Since the two-subband results have been understood rather well,[6,10] we thus emphasize density range where a three-subband model is warranted, that is when the lower excited subband 2 starts to be populated. We have chosen four densities, as denoted in the figures as well as in Table II. At the lowest one, the second subband is only thermally populated at 300 K, as witnessed by the appearance of the weak resonance from the lower excited subband 2 to the upper excited subband 3 (2→3) near 150 meV. Otherwise, only a single, inhomogeneously broadened resonance (1→2) is present. Expectedly, it is further weakened and

broadened thermally, as electrons increasingly populate higher energy states that have smaller transition energies, as displayed in Fig. 1. Increase in electron density strengthens resonance 2→3 because the amplitude of the resonance is roughly proportional to the density difference of the two subbands, $n_2 - n_3$. This dependence on the density difference also provides an explanation for the reduction in resonance strength as temperature rises at the four densities, which tends to deminish the difference. This is a phase space filling effect. Its another manifestation is seen in the red shift of resonance 1→2—more distinctly in Fig. 3—as a function of density. On the other hand, note that at certain density, 5×10^{12} cm^{-2} here, resonance 2→3 is temperature insensitive, which is a Coulomb collective effect. As we understand it now, ISBT is a collective phenomenon associated with the intersubband plasmon under normal circumstances, which could be a robust response, depending upon how strong the plasmon couples to the decay channels, such as through Landau damping.[12]

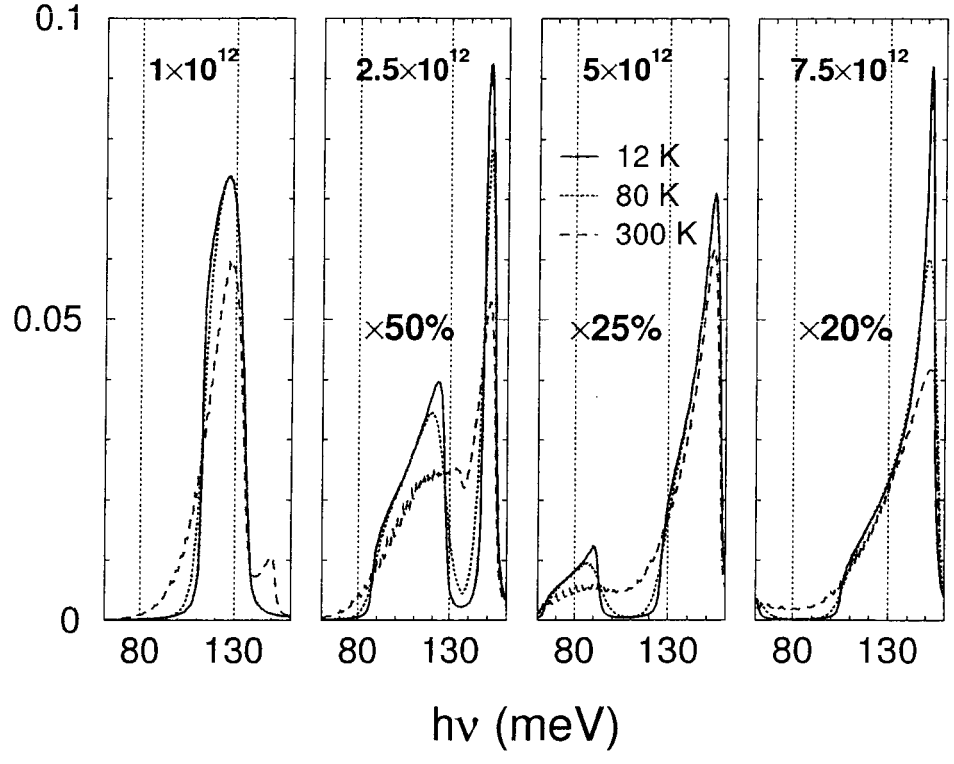

Figure 2. Absorbance evolution as a function of temperature at different electron densities. At low density, only the ground subband 1 is occupied and thus only single resonance (1→2) is observed at low temperature. Thermal population of the lowere excited subband 2 (see Table II) is revealed by the presence of a second resonance (2→3). This resonance grows as density increases. Accordingly, the first resonance is weakened and redshifted, as a consequence of phase space filling. Note that at certain density, like 5×10^{12} cm^{-2}, the second resonance is temperature insensitive.

The same results as in Fig. 2 are further presented as a function of electron density at different temperatures in Fig. 3 to illustrate all the effects from a different perspective. The phase space filling effects are more directly demonstrated in this case. First, at this particular QW thickness (15 nm), the first resonance line shape at the lowest chosen density of 1×10^{12} cm^{-2} is single-particle-like, or a spectrum reflecting the constant 2D joint density of states as a result of the interplay of collective excitations.[6] Increase in electron density has two consequences: starting populating the higher subband(s) and thus redistributing the oscillator strengths. As seen from resonance 1→2, a larger density broadens its line shape further, tilts it toward the high-frequency side, and redshifts the spectrum. All these are indications that the ISPs play a more dominant role in the interplay, which is expected for higher density cases. Then the resonance is gradually diminished as further increase in electron density actually decreases the density difference of the two subbands, $n_1 - n_2$. Also, more redshift

of the spectrum is observed. On the other hand, resonance 2→3 starts to appear below a density of 2×10^{12} cm^{-2} and takes a symmetric line shape at low temperature. This is changed as either the temperature or the density increases, as seen in the figure. Within the present three-subband model, further increase in electron density first blueshifts the spectrum before the upper subband begins to be populated, because the self-energy renormalization of the populated subband increases the effective intersubband separation—similar to the two-subband model results.[6] However, as expected, continuing increasing the electron density will start to populate the upper subband 3 (see Table II). Then, the oscillator strength will eventually decrease and the spectrum will redshift, just like resonance 1→2. Ultimately, we need to consider resonance(s) from subband 3 to even higher one(s). Note that we have not explicitly presented simulation results for resonance 1→3, which lies at higher energy that is beyond the scope of our interested spectral range, but its physics is fundamentally the same as what we have discussed with regard to the other two resonances.

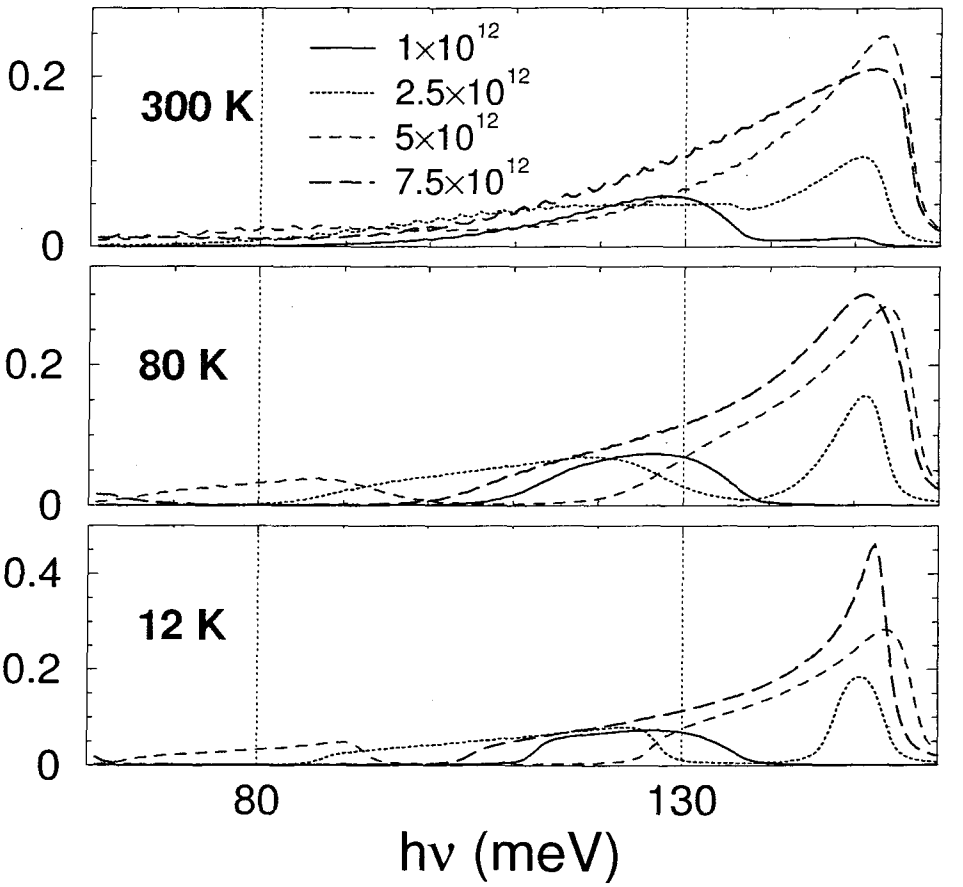

Figure 3. Same absorbance data as in Fig. 2, but presented as a function of electron density at different temperatures. Clearly seen is the phase space filling effects: Occupancy of the lower excited subband 2 introducing the second resonance (2→3) and adding to its oscillator strength as density increases; the enhancement of the plasmon peak at low temperature (12 K); redshifting both resonances as lower $\boldsymbol{k}$ states are occupied. Note the anomalous decrease at 300 K of the second resonance—a reflection of the robustness of the plasmon excitation: A phenomenon also observed by Warburton *et al.*.[12]

What has not been touched upon till now is the nonparabolicity effect, and this is the focus of Fig. 4. To demonstrate that, we choose an extreme case, that is to set the effective mass (m_3) of the upper excited subband equal to that (m_2) of the lower excited subband. In other words, there is no nonparabolicity effect, to the lowest order, for resonance 2→3 in the present case. Furthermore, the intersubband separation E_{23} is set to

173 meV, which bears no particular meaning other than to avoid the subject of the coupling of intersubband plasmons, which is the topic of a future paper. Not surprisingly, resonance 1→2 behaves as what have been shown previously. Furthermore, as expected, we observe narrow and symmetric Lorentzian line shape for resonance 2→3. Two features are worth noting: (i) an anomalous temperature dependence of the resonance at 2×10^{12} cm^{-2} and (ii) its temperature insensitivity at higher density. On the first feature, the resonance is strongly enhanced when temperature rises. This turns out to be a manifestation of the phase space filling effects: At low temperature, the second subband is populated with a rather small electron density. As the temperature increases, more electrons are thermally excited from the ground subband into the second one. As a result of this, the number of electrons available for absorbing incident photons at resonance 2→3 increases as well. Thanks to zero nonparabolicity, the temperature rise does not broaden the line shape, in contrast to a large nonparabolicity case as discussed already. Therefore, the anomalous temperature dependence of the resonance at the density of 2×10^{12} cm^{-2} is observed. Following the same line of thinking, the second feature of temperature insensitivity at higher density is easily understood. This also agrees with Warburton *et al.*.[12] Finally, the blueshift of the resonance with increase in electron density reflects an effect of the Hartree contribution in Eq. (3). It is often called the depolarization shift in literature[13,14] as, in the present case of zero nonparabolicity, it acts similar to a depolarization field.

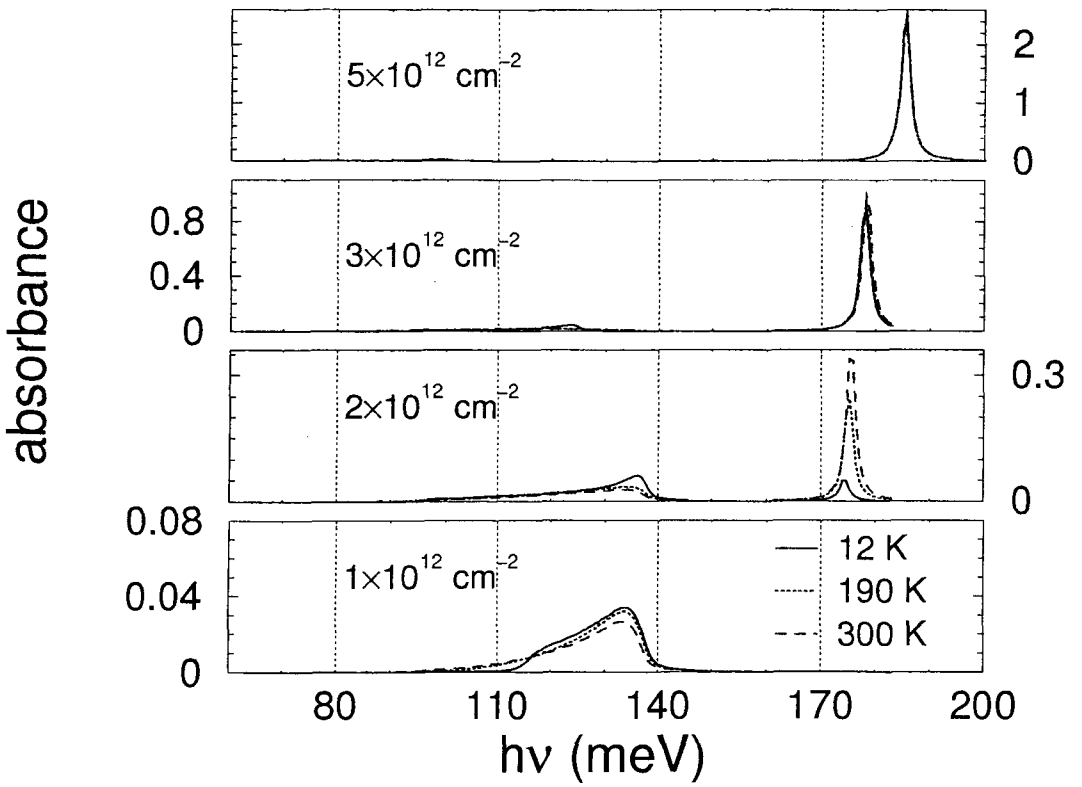

Figure 4. Absorbance evolution similar to Fig. 2, but depicting the nonparabolicity effect as the effective mass of the upper excited subband was set to equal that of the lower excited subband. The intersubband separation E_{23} is set to 173 meV. Two features are worth noting regarding the second resonance: (i) anomalous temperature dependence at 2×10^{12} cm^{-2} and (ii) its temperature insensitivity at higher density.

4. SUMMARY

In conclusion, we present a microscopic theoretical approach to intersubband optical resonances, similar to the semiconductor Bloch equations approach to interband transitions. This approach is applied to a 15 nm InAs quantum well case that is representative of materials with large conduction band nonparabolicity. The evolution of intersubband resonances as a function of the temperature and the electron density is presented and discussed in detail. We demonstrate the importance of the phase space filling effects and Coulomb many-body effects in understanding the underlying physics of intersubband resonances. Finally, we show that the nonparabolicity effect is instrumental in shaping the spectra of intersubband resonances.

ACKNOWLEDGMENTS

The work is supported by NASA contracts NAS 2-14303 and DTTS59-99-D-00437/A61812D to Advanced Management Technology Incorporated (AMTI), DARPA/AFOSR and NASA/NCI.

REFERENCES

1. H. C. Liu and F. Capasso, eds., *Intersubband Transitions in Quantum Wells: Physics and Device Application I*, vol. 62 of *Semiconductors and Semimetals*, Academic Press, San Diego, 2000; H. C. Liu and F. Capasso, eds., *Intersubband Transitions in Quantum Wells: Physics and Device Application II*, vol. 66 of *Semiconductors and Semimetals*, Academic Press, San Diego, 2000; R. Q. Yang, "Infrared laser based on intersubband transition in quantum well," *Superlattices Microstruct.* **17**, pp. 77–83, 1995.
2. O. Gauthier-Lafaye, P. Boucaud, F. H. Julien, S. Sauvage, S. Cabaret, J.-M. Lourtioz, V. Thierry-Mieg, and R. Planel, "Long-wavelength ($\approx$15.5 μm) unipolar semiconductor laser in GaAs quantum wells," *Appl. Phys. Lett.* **71**, pp. 3619–3621, 1997; I. Lyubomirsky, Q. Hu, and M. R. Melloch, "Measurement of far-infrared intersubband spontaneous emission from optically pumped quantum wells," *Appl. Phys. Lett.* **73**, pp. 3043–3045, 1998.
3. A. Liu and C. Z. Ning, "Near-infrared laser pumped intersubband THz laser gain in InGaAs-AlAsSb-InP quantum wells," *Appl. Phys. Lett.* **76**, pp. 1984–1986, 2000.
4. J. Li, K. I. Kolokolov, C. Z. Ning, D. C. Larrabee, G. A. Khodaparast, J. Kono, K. Ueda, Y. Nakajima, S. Sasa, and M. Inoue, "Intersubband transitions in InAs/AlSb quantum wells," in *Progress in Semiconductors II: Electronic and Optoelectronic Applications*, B. Weaver, M. O. Manasreh, C. Jagdishi, and S. Zollner, eds., *Proceedings of Materials Research Society* **744**, p. 571, 2003.
5. J. Li, K. I. Kolokolov, and C. Z. Ning, "Microscopic modeling of intersubband optical processes in type ii semiconductor quantum wells: Linear absorption," *Proc. SPIE* **4986**, p. 255, 2003.
6. J. Li and C. Z. Ning, "Interplay of collective excitations in quantum-well intersubband resonances," *Phys. Rev. Lett.* **91**, p. 097401, 2003.
7. J. Li, K. I. Kolokolov, C. Z. Ning, D. C. Larrabee, G. A. Khodaparast, J. Kono, K. Ueda, Y. Nakajima, S. Sasa, and M. Inoue, "Microscopic modeling of intersubband resonances in InAs/AlSb quantum wells," *Physica E* , 2003 (in press).
8. H. Haug and S. W. Koch, *Quantum Theory of the Electrical and Optical Properties of Semiconductors*, World Scientific, Singapore, 1994.
9. T. Kuhn, "Density matrix theory of coherent ultrafast dynamics," in *Theory of Transport Properties of Semiconductor Nanostructures*, E. Schöll, ed., Chapman & Hall, London, 1998. Chap. 6.
10. D. E. Nikonov, A. Imamoğlu, L. V. Butov, and H. Schmidt, "Collective intersubband excitations in quantum wells: Coulomb interaction versus subband dispersion," *Phys. Rev. Lett.* **79**, pp. 4633–4646, 1997.
11. K. I. Kolokolov, J. Li, and C. Z. Ning, "k.p hamiltonian without spurious-state solutions," *Phys. Rev. B* **68**, p. 161308(R), 2003.
12. R. J. Warburton, K. Weilhammer, C. Jabs, J. P. Kotthaus, M. Thomas, and H. Kroemer, "Collective effects in intersubband transitions," *Physica E* **7**, pp. 191–199, 2000.
13. T. Ando, A. B. Fowler, and F. Stern, "Electronic properties of two-dimensional systems," *Rev. Mod. Phys.* **54**, pp. 437–672, 1982.
14. M. Załużny, "Intersubband absorption line broadending in semiconductor quantum wells: Nonparabolicity contribution," *Phys. Rev.* **B**, pp. 4511–4514, 1991.

Microscopic Theory and Simulation of Quantum-Well Intersubband Absorption

Jianzhong Li and C. Z. Ning

Center for Nanotechnology and NASA Advanced Supercomputing Division
NASA Ames Research Center, Mail Stop N229-1, Moffett Field, CA 94035-1000

ABSTRACT

We study the linear intersubband absorption spectra of a 15 nm InAs quantum well using the intersubband semiconductor Bloch equations with a three-subband model and a constant dephasing rate. We demonstrate the evolution of intersubband absorption spectral line shape as a function of temperature and electron density. Through a detailed examination of various contributions, such as the phase space filling effects, the Coulomb many-body effects and the nonparabolicity effect, we illuminate the underlying physics that shapes the spectra.

Keywords: Intersubband transition, linear absorption, semiconductor heterostructure, InAs quantum well

1. INTRODUCTION

Study of semiconductor optoelectronic devices in the infrared regime attracts great attention owing to their applications in communications, sensing, imaging, and "finger printing" molecules. Current efforts of extending the spectral range of available light sources and detectors toward long micrometer wavelength regime involve very diverse device concepts and designs, such as quantum cascade lasers and type II interband lasers.[1] One of the promising device designs for achieving longwave infrared, or far-infrared lasing is based on optically pumped intersubband transitions (ISBTs).[2] The advantages of this concept include large dipole matrix elements and ultrafast dynamic response. Such design could be made even more attractive if material systems with deeper quantum wells (QWs) are adopted, such as the InGaAs/AlAsSb QWs, since then the pumping source for such systems could be another compact semiconductor diode laser.[3] In this respect, the antimonide-based QWs offer an interesting alternative, as the conduction band offset of InAs/AlSb heterostructure is as deep as 2 eV, providing more design flexibilities.

We have investigated effects of bandstructure, Coulomb interaction, electron-longitudinal optical (LO) phonon interaction, and other material-related issues on ISBTs within a two-subband model.[4–7] The analysis is based on density matrix formalism. In this paper, linear intersubband absorption spectra in a 15 nm InAs quantum well are studied in the same framework—the intersubband semiconductor Bloch equations approach—but under a three-subband model and dephasing rate approximation. We demonstrate the evolution of intersubband absorption line shape as temperature and carrier density are changed. Through a detailed examination of various contributions, such as phase space filling effects and Coulomb interaction-induced many-body effects, we elucidate the underlying physics that shapes the spectra.

Theoretical treatment of intersubband transitions typically involves two steps. The first step is to compute the bandstructure, while the second step is to formulate light-semiconductor interaction on the basis of this obtained bandstructure. The first step is sometimes called determination of the ground state, while the second step treats the excitations of the system by external light field. In the present model study, we model the bandstructure with different effective masses for the three parabolic subbands, whereas the density matrix theory[8,9] is adopted to treat the light-semiconductor heterostructure interaction. By explicitly formulating the two-point correlation functions, such as the intersubband polarization, the set of the so-called intersubband semiconductor Bloch equations (iSBEs) is derived. Within this approach, it is known that the exchange interaction leads to

Further author information: Both authors are employees of Computer Sciences Corporation.
J.L.: E-mail: jianzhng@nas.nasa.gov, Telephone: (650) 604 4410
C.Z.N.: E-mail: cning@mail.arc.nasa.gov, Telephone: (650) 604 3983

a self-energy renormalization (exchange self-energy, or XSE) to the single particle energy and a nonlocal vertex (excitonlike in the case of interband transitions) term that couples the other intersubband polarizations to each individual k-transition, whereas the direct (Hartree) interaction contributes the so-called depolarization field term that describes the dynamic screening of the charge carriers to the external exciting field, which is of collective nature and modifies the local field that each individual carrier feels. This paper detailedly examines the case of a 15 nm InAs quantum well within a three-subband model and illustrates how different contributions help shape the ISBTs as a function of temperature and carrier density.

This paper is organized as follows: In the second section, we summarize our theoretical considerations with a minimum set of equations; we present simulated ISBT spectra for the InAs quantum well in Sec. 3; and then we conclude the paper with a summary.

2. THEORETICAL CONSIDERATIONS

As mentioned above the microscopic theory consists of two steps: the static description of the subband dispersions and kinetic description for the intersubband optical transitions. We describe the energy dispersions in an approximate manner in this work, or more specifically, different effective masses are used for the three subbands. The focus of our work is on the kinetic description of the ISBTs.

To treat the light-semiconductor heterostructure interaction, we consider the following expectation values of the bilinear combination of creation ($c^{\dagger}_{n\boldsymbol{k}}$) and annihilation ($c_{n\boldsymbol{k}}$) operators among the same $\boldsymbol{k}$ (the in-plane electron wavevector) states within a three-subband model (subband labeled by index $n = 1, 2, 3$): ground subband population $f_{1\boldsymbol{k}} \equiv \langle c^{\dagger}_{1\boldsymbol{k}} c_{1\boldsymbol{k}} \rangle$, lower excited subband population $f_{2\boldsymbol{k}} \equiv \langle c^{\dagger}_{2\boldsymbol{k}} c_{2\boldsymbol{k}} \rangle$, upper excited subband population $f_{3\boldsymbol{k}} \equiv \langle c^{\dagger}_{3\boldsymbol{k}} c_{3\boldsymbol{k}} \rangle$, intersubband polarization $p^{12}(\boldsymbol{k}) \equiv \langle c^{\dagger}_{1\boldsymbol{k}} c_{2\boldsymbol{k}} \rangle$ between subband 1 and 2, $p^{23}(\boldsymbol{k}) \equiv \langle c^{\dagger}_{2\boldsymbol{k}} c_{3\boldsymbol{k}} \rangle$ between subband 2 and 3, $p^{13}(\boldsymbol{k}) \equiv \langle c^{\dagger}_{1\boldsymbol{k}} c_{3\boldsymbol{k}} \rangle$ between subband 1 and 3, and their corresponding Hermitian conjugates. Following the quantum kinetic approach, the semiclassical kinetic equations for the above dynamic variables are derived as a limiting case.[9] The derivation is extensive and will not be given here. The resultant equations (only the ones for intersubband polarizations here), under linearization with respect to the incident light field amplitude, some plausible assumptions, and the rotating wave approximation, are found as follows:

$$\left[\hbar\left(\omega + i\gamma_p^{mn}\right) - \left(\varepsilon_{n\boldsymbol{k}} - \varepsilon_{m\boldsymbol{k}}\right)\right] p_{\boldsymbol{k}}^{mn} = \left(\boldsymbol{d}_{\boldsymbol{k}}^{mn} \cdot \boldsymbol{E}_0 + \varepsilon_{\boldsymbol{k}}^{mn}\right)\left(f_{m\boldsymbol{k}} - f_{n\boldsymbol{k}}\right) - \sum_{j,\boldsymbol{q}} f_{j\boldsymbol{k}+\boldsymbol{q}}\left(V_{\boldsymbol{q}}^{njlj} p_{\boldsymbol{k}}^{ml} - V_{\boldsymbol{q}}^{ljmj} p_{\boldsymbol{k}}^{ln}\right) , \quad (1)$$

where ω is the angular frequency of the incident light of amplitude $\boldsymbol{E}_0$, γ_p^{mn} is the dephasing rate, $\boldsymbol{d}_{\boldsymbol{k}}^{mn}$ is the dipole matrix element, and $l \neq m$, $l \neq n$. $f_{m\boldsymbol{k}}$ is taken as the Fermi distribution function in the linear absorption calculation and $p_{\boldsymbol{k}}^{mn}$ is the amplitude of the intersubband polarization $p^{mn}(\boldsymbol{k})$. The renormalized single particle energy ($\varepsilon_{m\boldsymbol{k}}$) by the Coulomb self-energy and the *local field* correction term ($\varepsilon_{\boldsymbol{k}}^{mn}$) are, respectively, given by

$$\varepsilon_{m\boldsymbol{k}} = E_{m\boldsymbol{k}}^{(0)} - \sum_{l,\boldsymbol{q}} V_{\boldsymbol{q}}^{mlml} f_{l\boldsymbol{k}+\boldsymbol{q}} , \quad (2)$$

$$\varepsilon_{\boldsymbol{k}}^{mn} = -\sum_{j\neq l,\boldsymbol{q}} V_{\boldsymbol{q}}^{njml} p_{\boldsymbol{k}+\boldsymbol{q}}^{jl} + \sum_{j\neq l,\boldsymbol{q}} V_{\boldsymbol{0}}^{njlm} p_{\boldsymbol{q}}^{jl} . \quad (3)$$

The *local field* correction consists of a Fock (first) term that gives rise to a type of collective excitation called the repellon and a Hartree (second) term that stimulates another type of collective excitation called the intersubband plasmons (ISPs).[6,10] We mention that the first term is responsible for the Fermi-edge singularity effect, whereas the remaining term leads to the depolarization effect, as described detailedly in our earlier work. Their effects have been known from previous studies and play the same roles as well within the present three-subband model. The Coulomb matrix elements ($V_{\boldsymbol{q}}^{njml}$'s) are defined as in Ref..[5] The static single plasmon-pole approximation[8] has been used for screening the exchange interaction by the intrasubband processes in the present simulation work. The iSBEs are solved numerically by a matrix inversion for the intersubband polarization functions. We note that the last term in Eq. (1) is unimportant in this work.

The linear absorption coefficient is defined by

$$\alpha(\omega) \equiv \frac{\omega}{\varepsilon_0 n(\omega) c}\mathcal{I}m\{\epsilon(\omega)\} \approx \frac{\omega}{n(\omega)c}\mathcal{I}m\{\chi(\omega)\} , \quad (4)$$

with $n(\omega)$ being the background index of refraction (slowly varying in frequency), $\epsilon(\omega)$ the dielectric function, and c the speed of light *in vacuo*. The susceptibility, $\chi(\omega)$, is given by

$$\chi(\omega) \equiv P/\varepsilon_0 E_0 \,, \tag{5}$$

$$P = 2S/[(2\pi)^2 \mathcal{V}] \sum_{m \neq n} \int d\boldsymbol{k} \, \{d_{\boldsymbol{k}}^{mn}\}^* p_{\boldsymbol{k}}^{mn} \,. \tag{6}$$

where P is the total intersubband polarization, ε_0 is the electric constant, S is the QW area, and $\mathcal{V}$ is the QW volume. $\mathcal{V} = WS$, and W is the QW thickness. Finally, the absorbance of the semiconductor heterostructure is given by $2W\alpha(\omega)$ (per bounce at full TM polarization).

3. NUMERICAL RESULTS

Table I lists the bandstructure-related parameter values that were used in the numerical simulation. All the values were obtained using the spurious-state-free 8-band $\boldsymbol{k} \cdot \boldsymbol{p}$ Hamiltonian under the envelope function approximation,[5,11] with the exception of the depolarization factors. Their values are the quantum box results of the same QW thickness. In order for data integrity, the calculated subband populations are also presented here in Table II, which are auxillary to the understanding of the simulated spectra, as shown later.

Table I. Parameters used in simulations

subband effective mass	m_i (m_e)	0.0336 (1)	0.049 (2)	0.0715 (3)	
subband separation	E_{ij} (meV)	131.065 (12)	150.92 (23)	281.985 (13)	
dipole matrix element	d^{ij} (e·Å)	30.0 (12)	35.0 (23)	0.0 (13)	
depolarization factor	D^{jlmn} (W)	0.1222 (1122)	0.1146 (2233)	0.0343 (1133)	0.1101 (1232)

m_e: free electron mass; e: absolute electron charge. Numbers in parenthesis after entry values indicate subband indices. See Ref.[10] for definition of the depolarization factor.

The effective masses were found after a least square fitting to the $\boldsymbol{k} \cdot \boldsymbol{p}$ subbands; the subband separation is the energy difference at the Γ point ($\boldsymbol{k} = \boldsymbol{0}$) between the $\boldsymbol{k} \cdot \boldsymbol{p}$ subbands; the dipole matrix elements are found to be weakly dependent on the wavevector so that their values at the Γ point were used in the simulation. We mention that the depolarization factor is a measure of the contributing strength of the Hartree term to the *local field*, which in turn determines the strength of the ISPs.[6,10] Note that a value of the order of 0.1, in the unit of the QW thickness (W), means a rather strong depolarization effect; the total strength of the depolarization effect is proportional to the product of the QW thickness and the density difference between the subbands. Furthermore, coherent Coulomb effects due to the coupling of ISPs associated with individual ISBTs are important, and the results will be presented elsewhere.

Table II. Calculated subband populations

electron density (10^{12} cm^{-2})	temperature (K)	n_1	n_2	n_3
1.00	12	1.00	0.00	0.00
	80	1.00	2.41×10^{-5}	1.09×10^{-14}
	300	9.58×10^{-1}	4.16×10^{-2}	1.84×10^{-4}
2.50	12	2.11	3.92×10^{-1}	0.00
	80	2.10	3.95×10^{-1}	9.91×10^{-10}
	300	2.00	4.96×10^{-1}	3.49×10^{-3}
5.00	12	3.13	1.87	0.00
	80	3.13	1.87	3.77×10^{-5}
	300	3.09	1.84	6.78×10^{-2}
7.50	12	4.06	3.23	2.10×10^{-1}
	80	4.04	3.21	2.49×10^{-1}
	300	3.93	3.06	5.10×10^{-1}

n_i: Electron density in Subband i.

Shown in Fig. 1 are the energy dispersions of the considered three conduction subbands (left panel) and the single-particle absorption spectrum (right panel) of the 15 nm InAs QW. Owing to a nonparabolicity of the bulk InAs conduction band, dispersions for the three subbands are different: the subband separations are k-dependent. The rather strong nonparabolicity of InAs leads to a large value range of the intersubband separation. In a single-particle picture, this introduces an inhomogeneous broadening and an accompanying low frequency tailing to the absorption spectrum. All these are reflected in the figure. Note that we did not consider the temperature dependence of the subband strucuture in this model study. Also shown in the figure, as a comparison, is the case of vanishing nonparabolicity (dotted curves with upward arrows): The spectrum consists of sharp resonances without any inhomogeneous broadening.

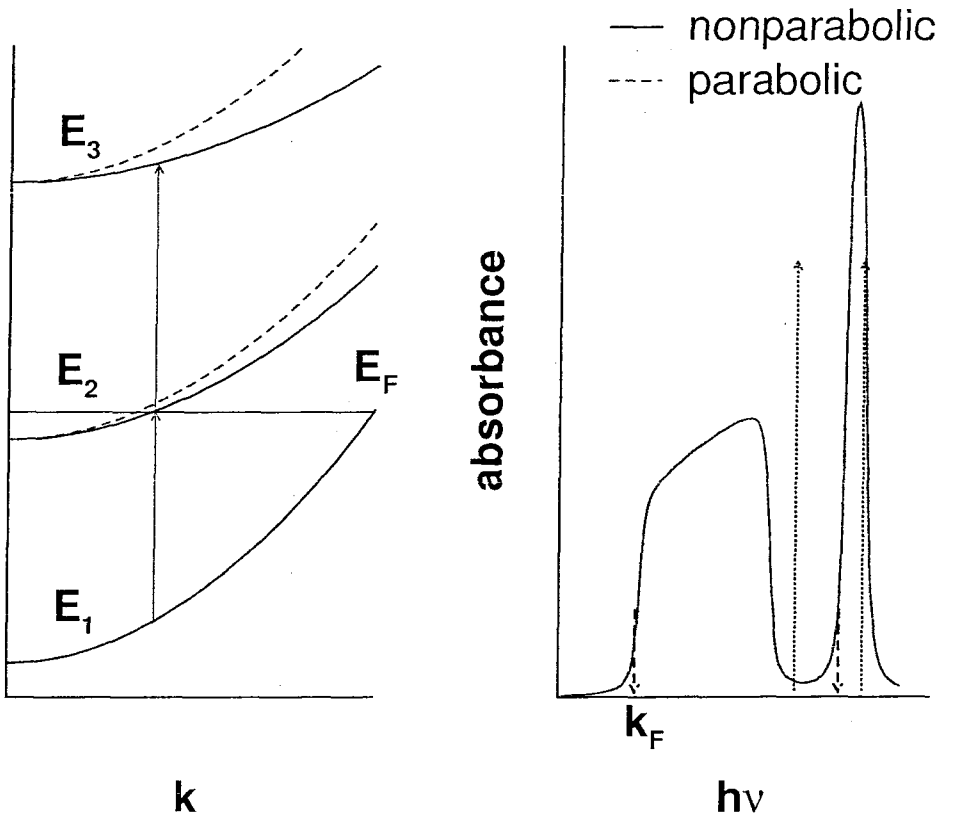

Figure 1. Schematic of subband dispersions (left panel) and single-particle intersubband absorption spectrum for a 15 nm InAs quantum well. The decreasing intersubband separation with increasing k represents the result of nonparabolicity in InAs conduction band, which is consequently and unambiguously reflected by the broadened absorption spectrum.

As outlined in Sec. 2, the matrix inversion method was used to solve Eq. (1) for the intersubband polarization functions. Then the absorbance was calculated using these functions according to Eqs. (4)–(6) and the results are presented in Figs. 2–4. We first show how the absorbance changes as a function of temperature at different electron densities in Fig. 2. Since the two-subband results have been understood rather well,[6,10] we thus emphasize density range where a three-subband model is warranted, that is when the lower excited subband 2 starts to be populated. We have chosen four densities, as denoted in the figures as well as in Table II. At the lowest one, the second subband is only thermally populated at 300 K, as witnessed by the appearance of the weak resonance from the lower excited subband 2 to the upper excited subband 3 (2→3) near 150 meV. Otherwise, only a single, inhomogeneously broadened resonance (1→2) is present. Expectedly, it is further weakened and

broadened thermally, as electrons increasingly populate higher energy states that have smaller transition energies, as displayed in Fig. 1. Increase in electron density strengthens resonance 2→3 because the amplitude of the resonance is roughly proportional to the density difference of the two subbands, $n_2 - n_3$. This dependence on the density difference also provides an explanation for the reduction in resonance strength as temperature rises at the four densities, which tends to deminish the difference. This is a phase space filling effect. Its another manifestation is seen in the red shift of resonance 1→2—more distinctly in Fig. 3—as a function of density. On the other hand, note that at certain density, 5×10^{12} cm^{-2} here, resonance 2→3 is temperature insensitive, which is a Coulomb collective effect. As we understand it now, ISBT is a collective phenomenon associated with the intersubband plasmon under normal circumstances, which could be a robust response, depending upon how strong the plasmon couples to the decay channels, such as through Landau damping.[12]

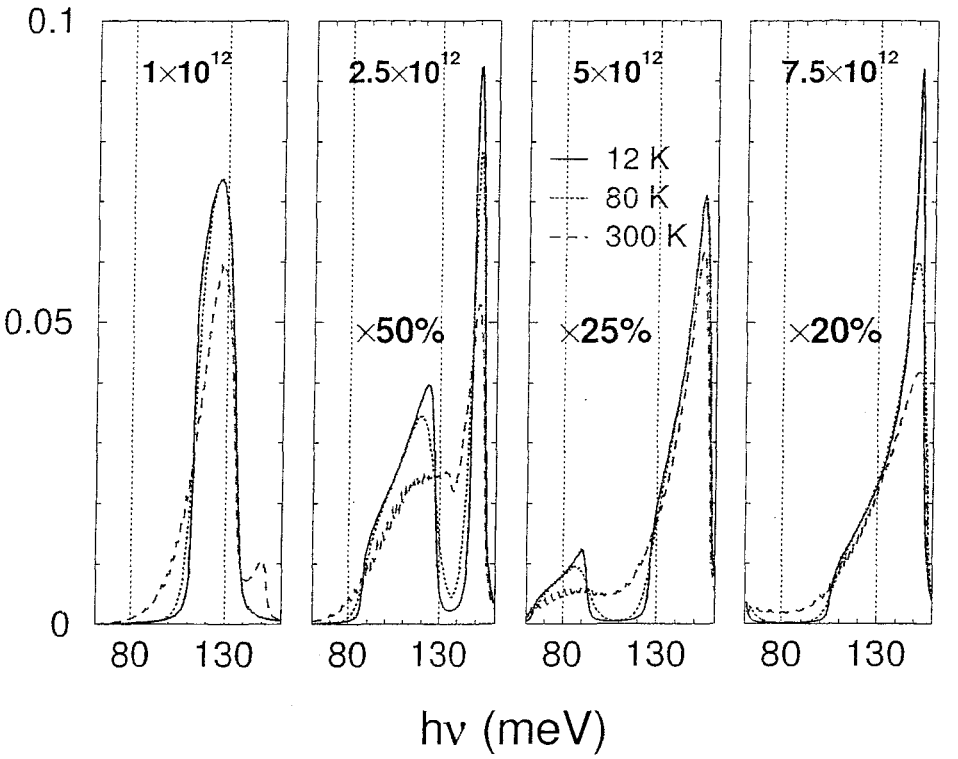

Figure 2. Absorbance evolution as a function of temperature at different electron densities. At low density, only the ground subband 1 is occupied and thus only single resonance (1→2) is observed at low temperature. Thermal population of the lowere excited subband 2 (see Table II) is revealed by the presence of a second resonance (2→3). This resonance grows as density increases. Accordingly, the first resonance is weakened and redshifted, as a consequence of phase space filling. Note that at certain density, like 5×10^{12} cm^{-2}, the second resonance is temperature insensitive.

The same results as in Fig. 2 are further presented as a function of electron density at different temperatures in Fig. 3 to illustrate all the effects from a different perspective. The phase space filling effects are more directly demonstrated in this case. First, at this particular QW thickness (15 nm), the first resonance line shape at the lowest chosen density of 1×10^{12} cm^{-2} is single-particle-like, or a spectrum reflecting the constant 2D joint density of states as a result of the interplay of collective excitations.[6] Increase in electron density has two consequences: starting populating the higher subband(s) and thus redistributing the oscillator strengths. As seen from resonance 1→2, a larger density broadens its line shape further, tilts it toward the high-frequency side, and redshifts the spectrum. All these are indications that the ISPs play a more dominant role in the interplay, which is expected for higher density cases. Then the resonance is gradually diminished as further increase in electron density actually decreases the density difference of the two subbands, $n_1 - n_2$. Also, more redshift

of the spectrum is observed. On the other hand, resonance 2—3 starts to appear below a density of 2×10^{12} cm^{-2} and takes a symmetric line shape at low temperature. This is changed as either the temperature or the density increases, as seen in the figure. Within the present three-subband model, further increase in electron density first blueshifts the spectrum before the upper subband begins to be populated, because the self-energy renormalization of the populated subband increases the effective intersubband separation—similar to the two-subband model results.[6] However, as expected, continuing increasing the electron density will start to populate the upper subband 3 (see Table II). Then, the oscillator strength will eventually decrease and the spectrum will redshift, just like resonance 1→2. Ultimately, we need to consider resonance(s) from subband 3 to even higher one(s). Note that we have not explicitly presented simulation results for resonance 1→3, which lies at higher energy that is beyond the scope of our interested spectral range, but its physics is fundamentally the same as what we have discussed with regard to the other two resonances.

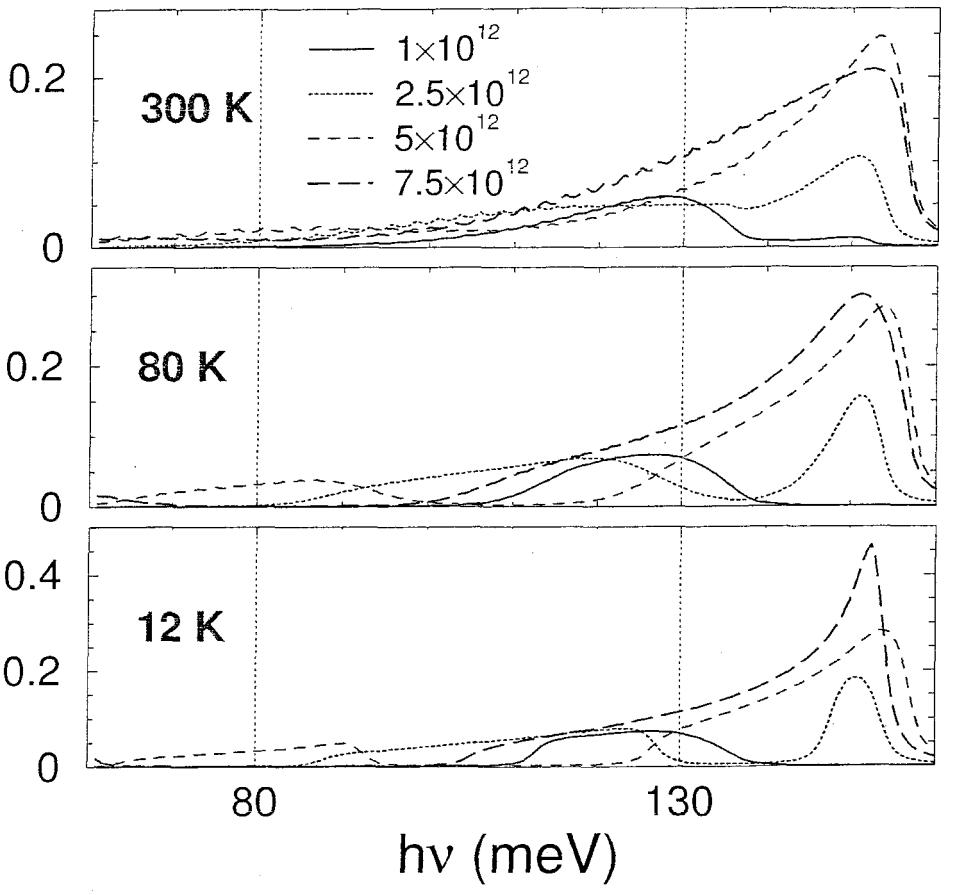

Figure 3. Same absorbance data as in Fig. 2, but presented as a function of electron density at different temperatures. Clearly seen is the phase space filling effects: Occupancy of the lower excited subband 2 introducing the second resonance (2→3) and adding to its oscillator strength as density increases; the enhancement of the plasmon peak at low temperature (12 K); redshifting both resonances as lower $\boldsymbol{k}$ states are occupied. Note the anomalous decrease at 300 K of the second resonance—a reflection of the robustness of the plasmon excitation: A phenomenon also observed by Warburton *et al.*.[12]

What has not been touched upon till now is the nonparabolicity effect, and this is the focus of Fig. 4. To demonstrate that, we choose an extreme case, that is to set the effective mass (m_3) of the upper excited subband equal to that (m_2) of the lower excited subband. In other words, there is no nonparabolicity effect, to the lowest order, for resonance 2→3 in the present case. Furthermore, the intersubband separation E_{23} is set to

173 meV, which bears no particular meaning other than to avoid the subject of the coupling of intersubband plasmons, which is the topic of a future paper. Not surprisingly, resonance 1→2 behaves as what have been shown previously. Furthermore, as expected, we observe narrow and symmetric Lorentzian line shape for resonance 2→3. Two features are worth noting: (i) an anomalous temperature dependence of the resonance at 2×10^{12} cm^{-2} and (ii) its temperature insensitivity at higher density. On the first feature, the resonance is strongly enhanced when temperature rises. This turns out to be a manifestation of the phase space filling effects: At low temperature, the second subband is populated with a rather small electron density. As the temperature increases, more electrons are thermally excited from the ground subband into the second one. As a result of this, the number of electrons available for absorbing incident photons at resonance 2→3 increases as well. Thanks to zero nonparabolicity, the temperature rise does not broaden the line shape, in contrast to a large nonparabolicity case as discussed already. Therefore, the anomalous temperature dependence of the resonance at the density of 2×10^{12} cm^{-2} is observed. Following the same line of thinking, the second feature of temperature insensitivity at higher density is easily understood. This also agrees with Warburton *et al.*.[12] Finally, the blueshift of the resonance with increase in electron density reflects an effect of the Hartree contribution in Eq. (3). It is often called the depolarization shift in literature[13,14] as, in the present case of zero nonparabolicity, it acts similar to a depolarization field.

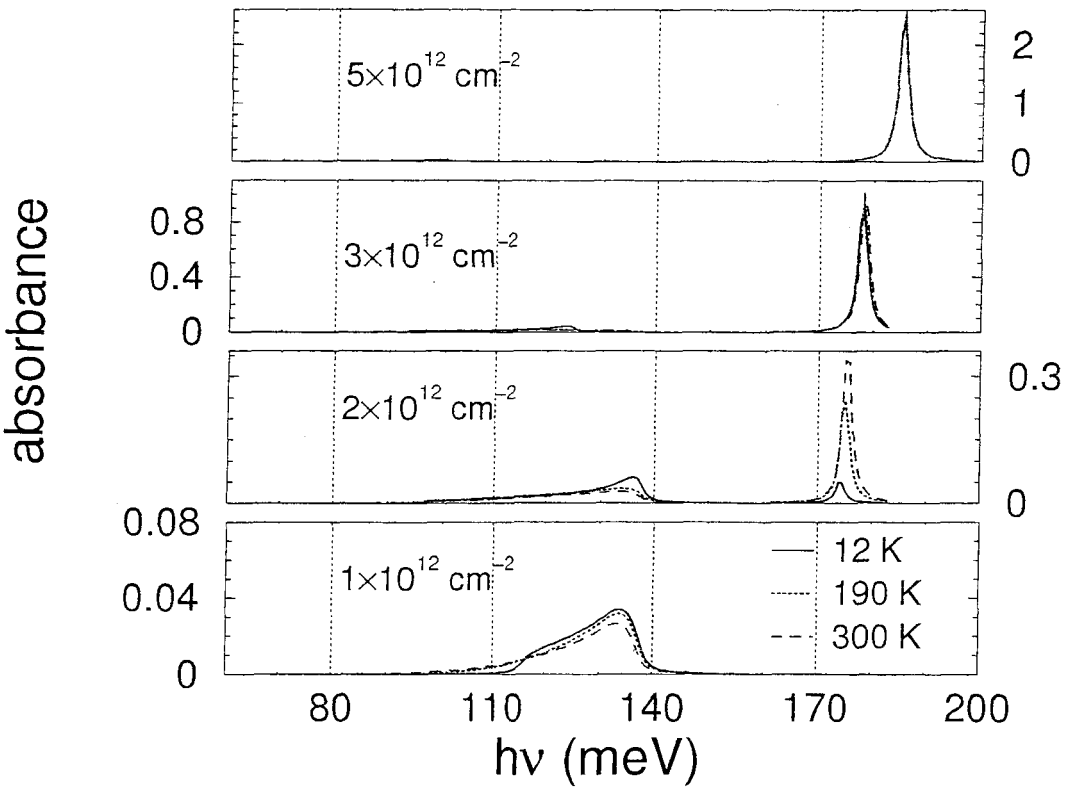

Figure 4. Absorbance evolution similar to Fig. 2, but depicting the nonparabolicity effect as the effective mass of the upper excited subband was set to equal that of the lower excited subband. The intersubband separation E_{23} is set to 173 meV. Two features are worth noting regarding the second resonance: (i) anomalous temperature dependence at 2×10^{12} cm^{-2} and (ii) its temperature insensitivity at higher density.

4. SUMMARY

In conclusion, we present a microscopic theoretical approach to intersubband optical resonances, similar to the semiconductor Bloch equations approach to interband transitions. This approach is applied to a 15 nm InAs quantum well case that is representative of materials with large conduction band nonparabolicity. The evolution of intersubband resonances as a function of the temperature and the electron density is presented and discussed in detail. We demonstrate the importance of the phase space filling effects and Coulomb many-body effects in understanding the underlying physics of intersubband resonances. Finally, we show that the nonparabolicity effect is instrumental in shaping the spectra of intersubband resonances.

ACKNOWLEDGMENTS

The work is supported by NASA contracts NAS 2-14303 and DTTS59-99-D-00437/A61812D to Advanced Management Technology Incorporated (AMTI), DARPA/AFOSR and NASA/NCI.

REFERENCES

1. H. C. Liu and F. Capasso, eds., *Intersubband Transitions in Quantum Wells: Physics and Device Application I*, vol. 62 of *Semiconductors and Semimetals*, Academic Press, San Diego, 2000; H. C. Liu and F. Capasso, eds., *Intersubband Transitions in Quantum Wells: Physics and Device Application II*, vol. 66 of *Semiconductors and Semimetals*, Academic Press, San Diego, 2000; R. Q. Yang, "Infrared laser based on intersubband transition in quantum well," *Superlattices Microstruct.* **17**, pp. 77–83, 1995.
2. O. Gauthier-Lafaye, P. Boucaud, F. H. Julien, S. Sauvage, S. Cabaret, J.-M. Lourtioz, V. Thierry-Mieg, and R. Planel, "Long-wavelength ($\approx$15.5 μm) unipolar semiconductor laser in GaAs quantum wells," *Appl. Phys. Lett.* **71**, pp. 3619–3621, 1997; I. Lyubomirsky, Q. Hu, and M. R. Melloch, "Measurement of far-infrared intersubband spontaneous emission from optically pumped quantum wells," *Appl. Phys. Lett.* **73**, pp. 3043–3045, 1998.
3. A. Liu and C. Z. Ning, "Near-infrared laser pumped intersubband THz laser gain in InGaAs-AlAsSb-InP quantum wells," *Appl. Phys. Lett.* **76**, pp. 1984–1986, 2000.
4. J. Li, K. I. Kolokolov, C. Z. Ning, D. C. Larrabee, G. A. Khodaparast, J. Kono, K. Ueda, Y. Nakajima, S. Sasa, and M. Inoue, "Intersubband transitions in InAs/AlSb quantum wells," in *Progress in Semiconductors II: Electronic and Optoelectronic Applications*, B. Weaver, M. O. Manasreh, C. Jagdishi, and S. Zollner, eds., *Proceedings of Materials Research Society* **744**, p. 571, 2003.
5. J. Li, K. I. Kolokolov, and C. Z. Ning, "Microscopic modeling of intersubband optical processes in type ii semiconductor quantum wells: Linear absorption," *Proc. SPIE* **4986**, p. 255, 2003.
6. J. Li and C. Z. Ning, "Interplay of collective excitations in quantum-well intersubband resonances," *Phys. Rev. Lett.* **91**, p. 097401, 2003.
7. J. Li, K. I. Kolokolov, C. Z. Ning, D. C. Larrabee, G. A. Khodaparast, J. Kono, K. Ueda, Y. Nakajima, S. Sasa, and M. Inoue, "Microscopic modeling of intersubband resonances in InAs/AlSb quantum wells," *Physica E* , 2003 (in press).
8. H. Haug and S. W. Koch, *Quantum Theory of the Electrical and Optical Properties of Semiconductors*, World Scientific, Singapore, 1994.
9. T. Kuhn, "Density matrix theory of coherent ultrafast dynamics," in *Theory of Transport Properties of Semiconductor Nanostructures*, E. Schöll, ed., Chapman & Hall, London, 1998. Chap. 6.
10. D. E. Nikonov, A. Imamoğlu, L. V. Butov, and H. Schmidt, "Collective intersubband excitations in quantum wells: Coulomb interaction versus subband dispersion," *Phys. Rev. Lett.* **79**, pp. 4633–4646, 1997.
11. K. I. Kolokolov, J. Li, and C. Z. Ning, "k.p hamiltonian without spurious-state solutions," *Phys. Rev. B* **68**, p. 161308(R), 2003.
12. R. J. Warburton, K. Weilhammer, C. Jabs, J. P. Kotthaus, M. Thomas, and H. Kroemer, "Collective effects in intersubband transitions," *Physica E* **7**, pp. 191–199, 2000.
13. T. Ando, A. B. Fowler, and F. Stern, "Electronic properties of two-dimensional systems," *Rev. Mod. Phys.* **54**, pp. 437–672, 1982.
14. M. Załużny, "Intersubband absorption line broadending in semiconductor quantum wells: Nonparabolicity contribution," *Phys. Rev.* **B**, pp. 4511–4514, 1991.